Planetary and Space Science 104 (2014) 173–184

Contents lists available at ScienceDirect

Planetary and Space Science

journal homepage: www.elsevier.com/locate/pss

Deriving the characteristics of warm electrons (100–500 eV) in the magnetosphere of Saturn with the Cassini Langmuir probe

P. Garnier [a,b,*], M.K.G. Holmberg [c], J.-E. Wahlund [c], G.R. Lewis [d,e], P. Schippers [f], A. Coates [d,e], D.A. Gurnett [g], J.H. Waite [h,*], I. Dandouras [a,b]

[a] Université de Toulouse; UPS-OMP; IRAP; Toulouse, France
[b] CNRS; IRAP; 9 Av. colonel Roche, BP 44346, F-31028 Toulouse cedex 4, France
[c] Swedish Institute of Space Physics, Box 537 SE 75121, Uppsala, Sweden
[d] Mullard Space Science Laboratory, Box 537 SE 75121, Uppsala, University College London, Dorking, United Kingdom
[e] The Centre for Planetary Sciences at UCL/Birkbeck, London, United Kingdom
[f] LESIA, Observatoire de Paris, Box 537 SE 75121, Uppsala, Meudon, France
[g] Department of Physics and Astronomy, University of Iowa, Iowa City, IA 52242, USA
[h] Space and Science Engineering Division, Southwest Research Institute, 6220 Culebra Rd., San Antonio, TX 78229, USA

ARTICLE INFO

Article history:
Received 22 April 2014
Received in revised form
25 July 2014
Accepted 15 September 2014
Available online 28 September 2014

Keywords:
Langmuir probe
Cassini
Electron density
Electron temperature
Energetic plasma
Pitch angle anisotropies

ABSTRACT

Though Langmuir probes (LP) are designed to investigate cold plasma regions (e.g. ionospheres), a recent analysis revealed a strong sensitivity of the Cassini LP measurements to hundreds of eV electrons. These warm electrons impact the surface of the probe and generate a significant current of secondary electrons, that impacts both the DC level and the slope of the current–voltage curve of the LP (for negative potentials) through energetic contributions that may be modeled with a reasonable precision.

We show here how to derive information about the incident warm electrons from the analysis of these energetic contributions, in the regions where the cold plasma component is small with an average temperature in the range ~[100–500] eV. First, modeling the energetic contributions (based on the incident electron flux given by a single anode of the CAPS spectrometer) allows us to provide information about the pitch angle anisotropies of the incident hundreds of eV electrons. The modeling reveals indeed sometimes a large variability of the estimated maximum secondary electron yield (which is a constant for a surface material) needed to reproduce the observations. Such dispersions give evidence for strong pitch angle anisotropies of the incident electrons, and using a functional form of the pitch angle distribution even allows us to derive the real peak angle of the distribution.

Second, rough estimates of the total electron temperature may be derived in the regions where the warm electrons are dominant and thus strongly influence the LP observations, i.e. when the average electron temperature is in the range ~[100–500] eV. These regions may be identified from the LP observations through large positive values of the current–voltage slope at negative potentials. The estimated temperature may then be used to derive the electron density in the same region, with estimated densities between ~0.1 and a few *particles*/cm^3 (cc). The derived densities are in better agreement with the CAPS measurements than the values derived from the proxy technique (Morooka et al., 2009) based on the floating potential of the LP. Both the electron temperature and the density estimates lie outside the classical capabilities of the LP, which are essentially $n_e > 5$ cc and $T_e < 5$ eV at Saturn. This approximate derivation technique may be used in the regions where the cold plasma component is small with an average temperature in the range ~[100–500] eV, which occurs often in the L range 6.4–9.4 R_S when Cassini is off the equator, but may occur anywhere in the magnetosphere. This technique may be all the more interesting since the CAPS instrument was shut down, and, though it cannot replace the CAPS instrument, the technique can provide useful information about the electron moments, with probably even better estimates than CAPS in some cases (when the plasma is strongly anisotropic).

Finally, a simple modeling approach allows us to predict the impact of the energetic contributions on LP measurements in any plasma environment whose characteristics (density, temperature, etc.) are known. LP observations may thus be influenced by warm electrons in several planetary plasma regions

* Corresponding author.
E-mail address: Philippe.Garnier@irap.omp.eu (P. Garnier).

http://dx.doi.org/10.1016/j.pss.2014.09.008
0032-0633/

in the solar system, and ambient magnetospheric electron density and temperature could be estimated in some of them (e.g. around several galilean satellites) through the use of Langmuir probes.

1. Introduction

Langmuir probes (Mott-Smith and Langmuir, 1926) are commonly used to investigate the cold plasma characteristics (e.g. electron temperature, density) in planetary ionospheres. The probe onboard the Cassini spacecraft – referred to as LP in the paper – is part of the Radio and Plasma Wave Science (RPWS) experiment (Gurnett et al., 2004), and provided detailed results not only about the Titan ionosphere (e.g. Wahlund et al., 2005a; Ågren et al., 2007; Garnier et al., 2009; Edberg et al., 2011; Ågren et al., 2012; Edberg et al., 2013), but also on the Saturnian plasma disk (Wahlund et al., 2005b; Morooka et al., 2009; Gustafsson and Wahlund, 2010; Holmberg et al., 2012) or dusty regions such as the Enceladus plume or the rings environment (Wahlund et al., 2009; Morooka et al., 2011; Sakai et al., 2013).

Langmuir probes' performances are limited for the derivation of the electron temperature and density: the temperature limit is due to the finite extent of the bias voltage U_B applied to the probe (e.g. $\pm$ 32 V for the Cassini LP), which cannot allow to see the whole distribution if the electron temperature is too large (i.e. above $\sim$5 eV for the LP in the Saturnian magnetosphere); the electron density limit is related to the photoelectrons from the spacecraft which hide the low plasma densities (below several cc or particles per cm^3).

Garnier et al. (2012) – hereafter G12 – however revealed a strong sensitivity of the Cassini LP measurements to the warm electrons (the adjective "warm" will refer to energies around hundreds of eV in this paper). The analysis of the ion side current (current for negative potentials) measured by the probe showed indeed a correlation with these warm electrons, which impact the surface of the probe and generate a significant current of secondary electrons. These warm electrons correspond to the peak energy of the secondary electron emission yield (SEEY) curve for the LP surface, and are mostly observed in the dipole L Shell range of $\sim$6–10 in the magnetosphere (DeJong et al., 2011).

Garnier et al. (2013) – hereafter G13 – then showed that both the DC level and the slope of the current–voltage curve of the LP (for negative potentials) are influenced by these warm electrons, through respective contributions called I_{ener} and b_{ener}. The authors managed to model both contributions, by using several approaches (empirical or theoretical), with a reasonable precision ($\sim$40% error).

The present work follows these two previous studies and aims at deriving information about the warm electrons from the analysis of the energetic contributions I_{ener} and b_{ener} to the current–voltage curve. We will first briefly describe the data used in our study (Section 2) and remind the theoretical modeling of the energetic contributions by G13 (Section 3). Then, we will show that modeling the energetic contributions reveals a strong sensitivity to the pitch angle anisotropies of the incident electrons (Section 4), and that the knowledge of these contributions also allows us to derive estimations of large electron temperatures (Section 5) and low electron densities (Section 6) in specific regions of the Saturnian magnetosphere. A last section (Section 7) will show how to predict the importance of the energetic contributions for LP measurements in any plasma environment, before a conclusion ends the paper (Section 8).

2. Description of the data

This work is based on the simultaneous usage of data from both the Cassini LP (Section 2.1; see Gurnett et al., 2004 for a general description of the probe characteristics) and CAssini Plasma Spectrometer experiments (Section 2.2; see Young et al., 2004 for a general description of CAPS). Only a short description of these data and of the extraction of the current due to the warm electrons will be provided below, we refer the readers to G13 for a detailed description.

2.1. The Cassini Langmuir probe data

The LP is a Titanium Nitride (TiN) coated conductive Titanium sphere, whose bias voltage (U_B) is actively applied to the LP with respect to the spacecraft in order to detect the electrons or ions, depending on the sign of the potential relative to the plasma ($U = U_B + V_{float}$, with V_{float} being the floating potential of the probe).

The derivation of the plasma parameters is performed through the fitting of the current–voltage (I–V) curve (Fahleson et al., 1974) using the Orbital Motion Limited (OML) theory Mott-Smith and Langmuir, 1926). We focus in this work on the ion side current (I_-) measured for a negative potential U.

G12 and G13 showed that, if we focus on regions off the equator – i.e. $Z > 2\ R_S$, with R_S=60,268 km the Saturn radius and (X, Y, Z) the Saturn centered equatorial coordinate system where Z points northward along Saturn's spin axis and X is in the Saturn equatorial plane positive towards the Sun – the currents induced by the presence of both charged dust and cold ions are small. The dust is indeed located near the equator, as well as the dominating water group ions that are centrifugally confined near the equator, Sittler et al., 2008). Both currents can thus be neglected compared with the photoelectron current (I_{ph}) due to the photoionization of the probe surface, and with the contribution due to the incident warm electrons ($I_{energet}$, which includes the incident, backscattered and induced secondary electrons).

The current for negative potentials I_- actually depends linearly on the bias potential at large negative U_B values (due to a current of incident ions proportional to the potential value), so that I_- is parametrized by a linear equation during the data analysis process:

$$I_- = m - bU_B \tag{1}$$

where m and b are respectively the DC level (corrected for the spacecraft attitude) and the slope of the fitted current–voltage curve on the ion side. These two parameters are the most important parameters of the LP for negative potentials, then used to derive the ion characteristics. G13 showed that the warm electrons impact both m and b, with contributions called respectively I_{ener} and b_{ener} (which thus correspond to the DC level and the slope of $I_{energet}$ the total current due to warm electrons) given by

$$I_{ener} = m + bV_{float} - I_{i_0} - I_{ph} \tag{2}$$

and

$$b_{ener} = b - b_{ions} \tag{3}$$

with I_{i_0} the "random ion current" due to incident ions, and b_{ions} the classic contribution of the ambient ions to the slope b of the current–voltage curve. As demonstrated by G13, both contributions due to ions (I_{i_0} and b_{ions}) are small when we focus on regions off the equator ($Z > 2\ R_S$), so that the energetic contributions I_{ener}

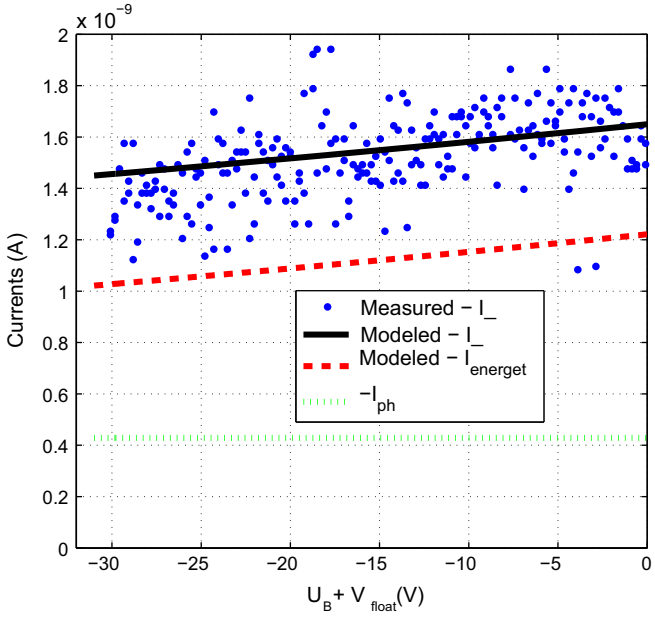

Fig. 1. (figure from Garnier et al., 2013) Negative potential side of the current–voltage curve obtained on 18 December 2007 at 21:13 UT. The total I_{-} current measured (blue dots) is compared with the I_{-} current modeled (black line) derived from the addition of the photoelectron current (I_{ph}, green line) and the current due to the energetic electrons ($I_{energet}$; with $n_e = 1.28\ \mathrm{cm}^{-3}$, $T_e = 173.5$ eV, $V_{float} = 0.62$ V and $\delta_{e_{max}} = 1.22$). The m and b parameters are respectively the intercept and the slope of the black line (i.e. the current I_{-}), while the energetic contributions I_{ener} and b_{ener} are respectively the intercept and the slope of the red line (i.e. the current $I_{energet}$). (For interpretation of the references to color in this figure caption, the reader is referred to the web version of this paper.)

and b_{ener} may be approximated by

$$\begin{cases} I_{ener} \approx m - I_{ph} \\ b_{ener} \approx b \end{cases} \tag{4}$$

Consequently, the knowledge of the slope and DC-level of the current–voltage curve (provided by the data analysis process), combined with the photoelectron current I_{ph} provided by Holmberg et al. (2012) at each time interval, allows us to extract the energetic contributions from the LP currents measured. An example of LP current–voltage curve inside the secondary electron current region is provided in Fig. 1. The current due to energetic particles is here the main current measured by the probe, leading to a clear positive value of the slope. The m/I_{ener} and b/b_{ener} parameters correspond to the intercept and the slope of the black/red lines (i.e. the $I_{-}/I_{energet}$ currents) respectively.

2.2. The Cassini CAPS ELS electron data

G13 demonstrated that the energetic contributions I_{ener} and b_{ener} may be modeled based on the knowledge of the incident electron distribution. We will focus here on the two theoretical methods, called "full distribution method" and "moments method". These methods need the respective following electron data from the CAPS-ELS instrument onboard Cassini:

- The full electron distribution made of the differential number fluxes $(\mathrm{keV\,cm^2\,sr\,s})^{-1}$ of all 63 CAPS-ELS energy channels from 0.53 eV/q (lower value of bin number 63) up to 28.3 keV/q (upper value of bin number 1).
- The 3D electron moments (density n_e, temperature T_e) derived by Lewis et al. (2008) assuming an isotropic Maxwellian distribution; since the lowest energy detected by CAPS is 0.6 eV, a threshold at 0.6 V or (to avoid checking for the number of counts measured) at 1 V is appropriate to avoid the data which cannot be trusted (G. Lewis, private communication).

Moreover, only the CAPS data from anode 5 are used, since it is the least affected by the spacecraft structures.

3. Modeling the energetic contributions I_{ener} and b_{ener}

This section summarizes (see in particular Section 5.1 in G13 for a detailed description) how the energetic contributions I_{ener} and b_{ener} may be modeled, using either the full distribution or the moments method. The current $I_{energet}$ induced by the presence of warm electrons (and of subsequent backscattered and secondary electrons) may be given according to Lai and Tautz (2008) by

$$I_{energet} = \frac{2\pi e}{m_e^2} A_{LP} \int_0^{\infty} E f_{ie}(E)(1-\delta_e(E)-\eta_e(E))\, dE * e^{eU/k_B T_e} \tag{5}$$

with m_e being the electron mass, A_{LP} the surface of the spherical probe (whose radius is 0.025 m), E the incident electron energy, f_{ie} the incident electron distribution function, δ_e the SEEY function for the LP surface, η_e the backscattering coefficient and k_B the Boltzmann constant.

We chose the SEEY function of Sanders and Inouye (1978): $\delta_e(E) = c(e^{-E/a} - e^{-E/b})$ with $a = 4.3E_M$, $b = 0.367E_M$ and $c = 1.37\delta_{e_{max}}$, where E_M is the peak energy of the SEEY curve (~ 350 eV, see G12) and $\delta_{e_{max}}$ is the maximum yield value. The literature provides a large possible range of values for $\delta_{e_{max}}$ (i.e. 1.1–2.4, see Baglin et al., 2000; He et al., 2001; Walters and Ma, 2001; Lorkiewicz et al., 2007) for surface compositions similar to the Cassini LP, but G13 managed to estimate more precisely the most appropriate values depending on the method (full distribution or moments) used and on the dataset selection considered.

The backscattering coefficient was taken constant at $\eta_e = 0.3$ based on Monte Carlo simulations (M. Belhadj, French Aerospace Laboratory, private communication) for TiN surfaces which give $\eta_e(E) \approx 0.2$–0.4.

Eq. (5) does not include explicitly the angular dependance. This equation was however used for the following reasons: (1) G13 showed that it was appropriate to reproduce the LP observations, (2) this simple expression will allow us to derive analytical expressions to estimate the electron moments (T_e and n_e, see Sections 5 and 6), and (3) the incident electron angular distribution is often poorly known (see Section 4 for a detailed investigation).

The energetic current $I_{energet}$ impacts both the m and b parameters derived during the LP data analysis respectively through the I_{ener} and b_{ener} contributions. They are thus respectively the DC level and the slope of the $I_{energet}$ current, calculated over the range of potentials $U_B = [-32\ \mathrm{V} - 5\ \mathrm{V}]$:

$$b_{ener} = -\frac{I_{energet}(U_B = -5\ \mathrm{V}) - I_{energet}(U_B = -32\ \mathrm{V})}{-5+32} \tag{6}$$

and

$$I_{ener} = \frac{\int_{U_B=-32}^{U_B=-5} (I_{energet}(U_B) + b_{ener} U_B)\, dU_B}{-5+32} \tag{7}$$

Two different methods may then be used to include the distribution function f_{ie} of incident electrons (needed in Eq. (5)), since one can use

- the full energy distribution of the incident electrons measured, given by $f_{ie}(E) \sim 5m_e^2 DNF(E)/eE$, where $DNF(E)$ is the initial differential number fluxes $(\mathrm{keV}^{-1}\,\mathrm{cm}^{-2}\,\mathrm{sr}^{-1}\,\mathrm{s}^{-1})$ measured in each of the 64 energy channels of CAPS-ELS

- the Maxwellian distribution based on the electron moments n_e and T_e: $f_{ie} = n_e(m_e/2\pi k_B T_e)^{3/2} e^{-E/k_B T_e}$

The full distribution method then leads, after easy calculations detailed in Section 5.1 of G13, to

$$\begin{cases} I_{ener_{full}} = -\dfrac{10\pi A_{LP} A\left(\dfrac{k_B T_e}{e} - 37/2\right)}{27} \int_0^\infty DNF(E)(1-\delta_e(E)-\eta_e(E))\, dE \\ b_{ener_{full}} = -\dfrac{10\pi A_{LP} A}{27} \int_0^\infty DNF(E)(1-\delta_e(E)-\eta_e(E))\, dE \end{cases} \tag{8}$$

with

$$A = \frac{2}{27} e^{e(V_{float} - 37/2)/k_B T_e} \sinh\left(\frac{27e}{2k_B T_e}\right) \tag{9}$$

where sinh is the hyperbolic sinus function

The moments method leads to

$$\begin{cases} I_{ener_{moments}} = \dfrac{A n_e K L\left(\dfrac{k_B T_e}{e} - 37/2\right)}{27} \\ b_{ener_{moments}} = -\dfrac{A n_e K L}{27} \end{cases} \tag{10}$$

with

$$K = \sqrt{\frac{k_B T_e}{2\pi m_e}} A_{LP} e \tag{11}$$

$$L = 1 - \eta_e + \frac{cb^2}{(b + k_B T_e)^2} - \frac{ca^2}{(a + k_B T_e)^2} \tag{12}$$

Since the maximum yield $\delta_{e_{max}}$ is poorly known for the LP surface from the literature (as detailed above), G13 derived expressions allowing to estimate the $\delta_{e_{max}}$ value needed to reproduce exactly the measured energetic contributions $I_{ener_{meas}}$ or $b_{ener_{meas}}$ at each time interval. These expressions are easily derived from Eq. (8), since $\delta_e(E)$ is directly proportional to $\delta_{e_{max}}$:

$$\begin{cases} \delta_{e_{max_{Iener}}} = \dfrac{\dfrac{A\left(\dfrac{k_B T_e}{e} - 37/2\right)}{27} \dfrac{2\pi e}{m_e^2} A_{LP} \int_0^\infty Ef_{ie}(E)(1-\eta_e)\, dE - I_{ener_{meas}}}{\dfrac{A\left(\dfrac{k_B T_e}{e} - 37/2\right)}{27} \dfrac{2\pi e}{m_e^2} A_{LP} \int_0^\infty Ef_{ie}(E) \dfrac{\delta_e(E)}{\delta_{e_{max}}}\, dE} \\ \delta_{e_{max_{bener}}} = \dfrac{\dfrac{-A}{27} \dfrac{2\pi e}{m_e^2} A_{LP} \int_0^\infty Ef_{ie}(E)\, dE - b_{ener_{meas}}}{\dfrac{-A}{27} \dfrac{2\pi e}{m_e^2} A_{LP} \int_0^\infty Ef_{ie}(E) \dfrac{\delta_e(E)}{\delta_{e_{max}}}\, dE} \end{cases} \tag{13}$$

with the incident electron distribution function f_{ie} which may be calculated either from the full distribution or from the electron moments.

4. Investigating the incident electrons pitch angle anisotropies

We will show in this section how the modeling of the energetic contributions I_{ener} and b_{ener} reveals a strong sensitivity to the pitch angle anisotropies of the incident energetic ($\sim$250–450 eV) electrons.

Fig. 2 shows an analysis of the following period: 16:00–18:00 UT on December 19, 2007. The spacecraft was located inside the secondary electron current region identified by G12 and off the equator, with L Shell values from 8.58 to 9.46 and Z values from -2.17 R_S to -2.12 R_S. The top two panels give the CAPS ELS pitch angle spectrogram for the 253–474 eV electrons, with all the eight anodes (panel (a)) and only the anode 5 (panel (b)). The pitch angle distribution (PAD) is thus strongly anisotropic and always peaks near 180°. If we focus on the anode 5 only, the same anisotropy may be seen, with larger fluxes at larger pitch angles.

We first extracted the energetic contributions I_{ener} and b_{ener} during this period. We then calculated the values of $\delta_{e_{max}}$ needed at each time interval to reproduce the observed I_{ener} or b_{ener}, as given by Eq. (13), for both the full distribution and moments methods. The panel (c) in Fig. 2 compares some of these estimated maximum yield values and the pitch angle of anode 5 during the 2 h period. A clear anti-correlation may be seen between the pitch angle and the $\delta_{e_{max}}$ values, in particular for the I_{ener} full distribution method. Pearson's correlation factors (Press et al., 2007) are indeed negative: $-0.37/-0.32$ $/-0.87$ for the respective I_{ener} moments/b_{ener} moments/I_{ener} full distribution methods.

The modeling of the energetic contributions indeed includes the incident electron distribution given by the anode 5 of CAPS ELS. When this anode is scanning through an anisotropic PAD, the measured flux often does not correspond to the omnidirectional flux that actually impacts the LP and generates secondary electrons. The LP collects electrons from all directions, and is thus sensitive to the flux integrated over all pitch angles. The maximum yield values estimated in Fig. 2 panel (c) should theoretically always be constant, i.e. at the value corresponding to the surface composition of the LP. The variability of the estimated $\delta_{e_{max}}$ and its anti-correlation with the pitch angle variability of anode 5 reveals that the pitch angle distribution of the incident warm electrons is anisotropic. If we used in the modeling equations the omnidirectional fluxes actually impacting the LP, the estimated $\delta_{e_{max}}$ would be constant during the period considered. Strong anisotropies will thus lead to large dispersions of the estimated $\delta_{e_{max}}$.

Another way may be used to confirm this assessment and show that even more information may be derived about the PAD of the incident electrons. We propose to apply to the measured fluxes/distribution an ad hoc weighting function W that takes into account the pitch angle anisotropy of the electrons, in order to derive an estimate of the omnidirectional fluxes/distribution (i.e. $f_{ie,omni} = f_{ie,anode5} * W$). The following weighting function is considered:

$$W(\alpha_{PAD}, n, r) = \frac{1}{(1 + r\ \cos(|\alpha_{an5} - \alpha_{PAD}|))^n} \tag{14}$$

where n and r are free parameters (with $0 < r < 1$), α_{an5} is the pitch angle of the anode 5 and α_{PAD} is the peak angle of the pitch angle distribution ($\sim 180°$ from the CAPS pitch angle spectrogram in Fig. 2).

The weighting function given by Eq. (14), when multiplied by the anode 5 incident electron distribution function f_{ie} and if the peak angle α_{PAD} is known, allows us to roughly derive the omnidirectional flux for an anisotropic PAD. This weighting function will indeed on the one side reduce the fluxes measured by the anode 5 when its pitch angle α_{an5} is close to the peak angle of the PAD α_{PAD}, and it will on the other side enhance the fluxes when α_{an5} and α_{PAD} are very different. Our function is more complex than the $\sin(\alpha)^n$ function used by several authors (e.g. Rymer et al., 2008), but this function would lead to unphysical fluxes when $\sin(\alpha) \sim 0$.

Fig. 3 shows the impact of such a weighting on the variability of the estimated $\delta_{e_{max}}$ values. The left panel gives the dispersion of the maximum yields estimated – during the same time period as in Fig. 2 – that are needed to reproduce the measured I_{ener} parameter with the moments method, after a weighting of the electron distribution function f_{ie}. The dispersion is given as a function of both the index n and the peak angle α_{PAD} assumed (with $r = 0.5$). The dispersion of the estimated maximum yield is

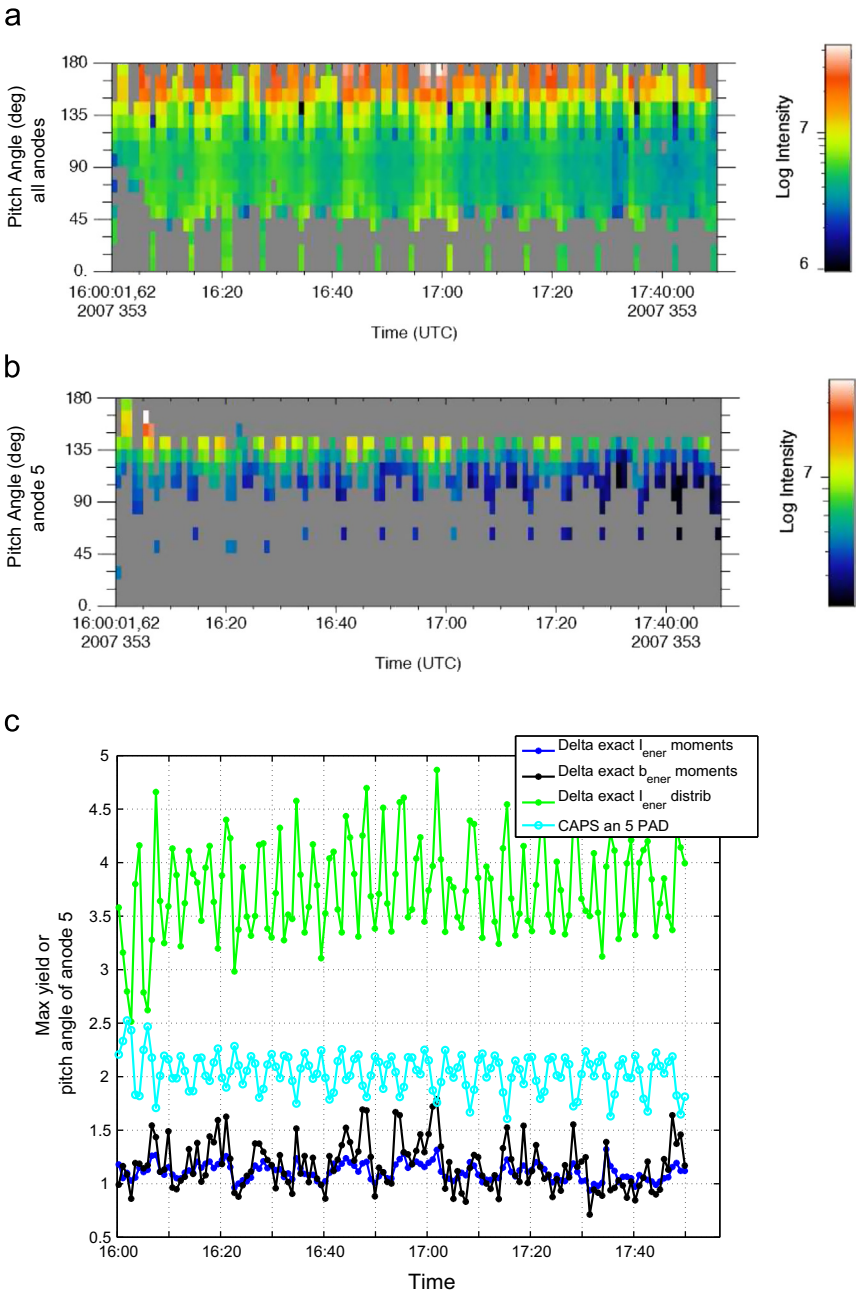

Fig. 2. Panel (a): pitch angle spectrogram for the 253–474 eV electrons with all anodes included, as a function of time on 2007 December 19; the color bar shows the differential number flux (keV cm^2 sr s)$^{-1}$ at these energies (i.e. averaged over the CAPS ELS channels 34–37). Panel (b): same as panel (a), with only the anode 5. Panel (c): comparison between the pitch angle time profile of anode 5 (same profile as panel (b) but with angle values divided by 30 for an easier comparison) and the values of the maximum yield $\delta_{e_{max}}$ estimated from several methods: from the moments or full distribution approach, from the I_{ener} or b_{ener} parameter. (For interpretation of the references to color in this figure caption, the reader is referred to the web version of this paper.)

thus minimum if we assume a peak angle of the PAD near $\sim 180^\circ$ as observed, and for large index n values.

The right panel corresponds to similar results in 1D, where we use a fixed value $n=2$ as an example and compare between various methods (using I_{ener} or b_{ener}, the full distribution or moments methods). All three dispersion profiles (i.e. all three methods used) show the same behavior during this 2 h time interval, with a minimum dispersion if the peak angle of the PAD is assumed to be close to $\sim 180^\circ$. Moreover, the dispersion values obtained after an appropriate weighting (i.e. assuming α_{PAD} close to $\sim 180^\circ$) of the incident electron distribution are smaller than the dispersion observed without any weighting: this means that a significant part of the variability observed for the estimated $\delta_{e_{max}}$ (without any weighting) is due to an incomplete distribution given by the anode 5, which provides variable fluxes different from the omnidirectional fluxes impacting the LP: the PAD is strongly anisotropic, and the anode 5 scans through it so that the fluxes measured are highly variable (by a factor of 5–10) and are often low compared with the fluxes averaged over all anodes. The observed dispersion is reduced by about 35–40% after an appropriate weighting during this period. As a consequence, a significant part of the 40% relative error between the modeled and measured energetic contributions discussed by G13 is thus probably related to the presence of PAD anisotropies of the warm electrons that are not properly taken into account when using the single CAPS anode 5 (depending on its exact orientation).

The LP alone cannot provide any information about the PAD of the incident energetic ($\sim$ 250–450 eV) electrons. Such anisotropies

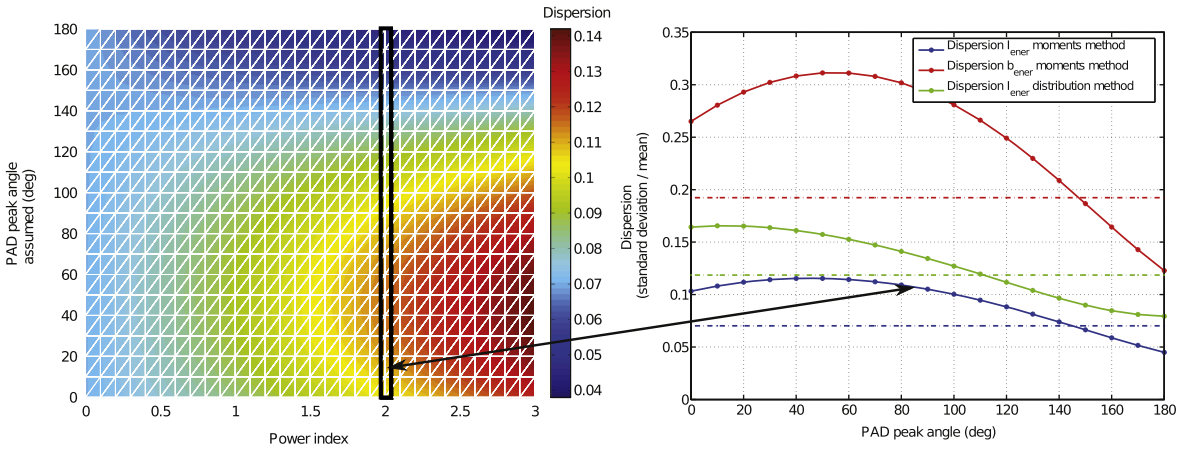

Fig. 3. Left panel: dispersion (i.e. standard deviation/mean value, given by the color bar) of the estimated values for the maximum yield $\delta_{e_{max}}$ – from the weighted moments method using the I_{ener} parameter during the time interval of Fig. 2 (2007 December 19, 16:00–17:50) – as a function of both the PAD peak angle α_{PAD} and the power index n assumed for the weighting in Eq. (14). Right panel: examples of dispersion profiles for the estimated $\delta_{e_{max}}$ values from several methods (including the profile from the left panel), with (solid lines) or without (dashed lines) using the weighting function for the PAD of the incident electrons; the weighted profiles assume $n=2$. See text for more details. (For interpretation of the references to color in this figure caption, the reader is referred to the web version of this paper.)

will thus not be directly visible in the LP current-voltage curve. However, the modeling of the energetic contributions I_{ener} and b_{ener}, based on the incident electron distribution function (that is sensitive to anisotropies) given by the CAPS ELS anode 5, reveals a strong sensitivity to the pitch angle anisotropies. Large dispersions of the estimated $\delta_{e_{max}}$ (needed to reproduce the observed I_{ener} or b_{ener}) give evidence for strong pitch angle anisotropies. If the exact maximum yield of the LP surface was known, one could even in principle derive the omnidirectional fluxes of these electrons at each time interval, whatever the pitch angle coverage of the CAPS instrument is. When the PAD anisotropy is stable during a certain time period (as in Fig. 2), it is also possible to roughly estimate the peak angle of the PAD. Besides, this study shows that the PAD anisotropies (and the usage of the single CAPS anode 5) may contribute significantly to the error between measurements and modeling of the energetic contributions discussed by G13.

5. Deriving large electron temperatures

We will show in this section that large electron temperatures may be derived in the regions where the energetic current $I_{energet}$ – induced by the presence of warm electrons – is significant.

In such regions, combining the theoretical expressions (with the moments method) for the respective DC level and slope energetic contributions I_{ener} and b_{ener}, given by Eq. (10), leads to

$$\frac{I_{ener}}{b_{ener}} = \frac{k_B T_e}{e} - 37/2 \tag{15}$$

or

$$T_{e_{eV}} = \frac{I_{ener}}{b_{ener}} + 37/2 \tag{16}$$

This simple expression suggests the possibility to derive Maxwellian electron temperatures in the regions where the warm electrons (100–500 eV electrons) have a significant influence on the LP observations. This would enlarge the LP capabilities regarding the electron temperature measurement, which is usually limited by the extent of the voltage sweep (i.e. to electron temperatures below $\sim$5–10 eV in the magnetosphere).

This capability will first be analyzed based on the following case studies:

(a) 2008 May 18, 01:40–02:10 UT: This period was analyzed in our previous papers (see G12 or G13) and reveals the influence of a PAD anisotropy; the L Shell is between 7.0 and 9.6 and $|Z|$ is above 2.4 R_S.
(b) 2007 December 19, 16:00–17:50 UT: This period was analyzed in Section 4.
(c) 2008 April 30, 06:08–07:25 UT: The L Shell is between 7.0 and 9.0 and $|Z|$ is above 2.6 R_S.
(d) 2008 May 25, 18:53–19:25 UT: The L Shell is between 7.2 and 9.0 and $|Z|$ is above 2.7 R_S.

The energetic contributions I_{ener} and b_{ener} were derived during the four periods, as described in Section 2.1, leading to the estimated electron temperature using Eq. (16). Fig. 4 shows the comparison between the measured and estimated electron temperatures during the four periods. Half of the data correspond to spacecraft potential values above 0.6 V (i.e. the low-energy threshold of CAPS ELS), which should however not much impact the measurements given the large electron temperature during the time intervals. Low positive values (below 2×10^{-3} nA/V) of the slope b of the current–voltage curve (defined in Eq. (1)) are encountered during a part of the two first periods.

The estimated temperature is thus very close to the measured temperature, all the more for the time steps where the slope b of the current–voltage curve was large. Large slope values correspond to a strong influence of the warm electrons (as shown by G13), and thus to an expected good estimation of the electron temperature from the ratio I_{ener}/b_{ener}. The relative absolute errors between the estimated (for $b>2\times10^{-3}$ nA/V) and measured electron temperatures are, for the four periods, of about 76% (panel (a)), 29% (panel (b)), 18% (panel (c)) and 24% (panel (d)).

The largest error corresponds to a period (i.e. 2008 May 18, 01:40–02:10 UT) where the anode 5 of the CAPS ELS instrument was scanning through a probably anisotropic PAD, leading to a modulation of the electron temperature derived from this anode measurements. The anode 5 pitch angle was indeed varying sinusoidally and is strongly anti-correlated with the electron temperature profile measured (as well as the electron density, see Fig. 6). The pitch angle coverage (combining all anodes) was however too small during this period to investigate in detail the anisotropy issue as in Section 4.

Beyond these case studies, a statistical analysis was also performed based on the LP data from February 1, 2005 to July 30, 2008 (with more than 250,000 time intervals) previously used by G13. Fig. 5 shows the mean ratio between the estimated and the measured electron temperature, for different sub-selections of

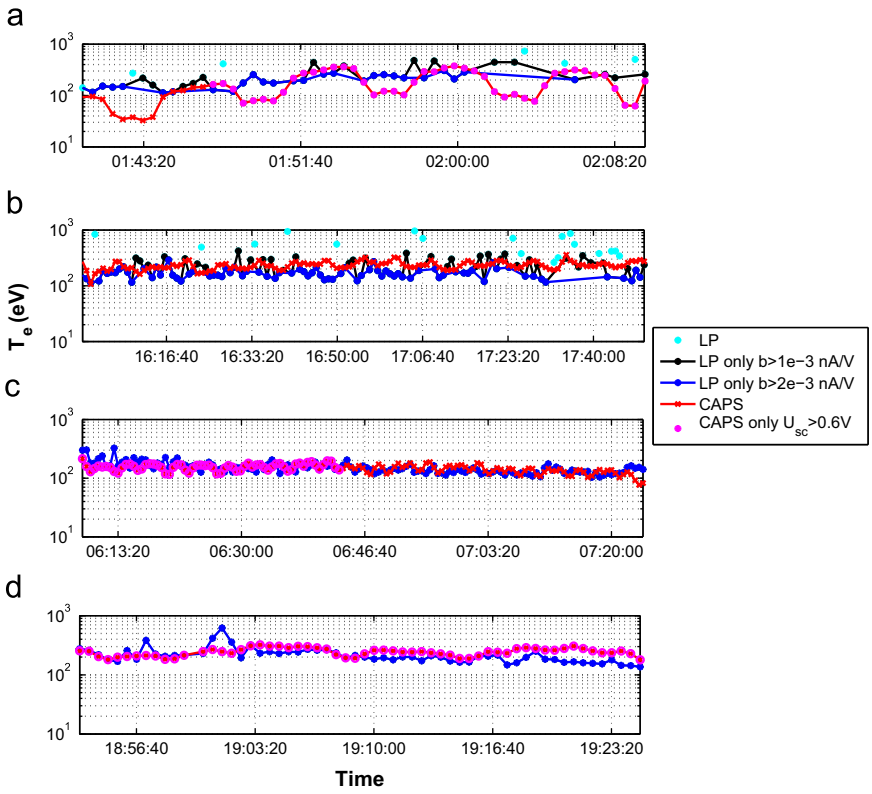

Fig. 4. Electron temperature T_e during several case studies: 2008 May 18, 01:40–02:10 UT (panel (a)), 2007 December 19, 16:00–17:50 UT (panel (b)), 2008 April 30, 06:08–07:25 UT (panel (c)) and 2008 May 25, 18:53–19:25 UT (panel (d)). The temperatures measured by CAPS ELS (with or without a spacecraft potential above 0.6 *V*) are compared with the temperatures estimated from the ratio I_{ener}/b_{ener} measured by the LP (Eq. (16)), for several data selections based on the slope *b* values measured.

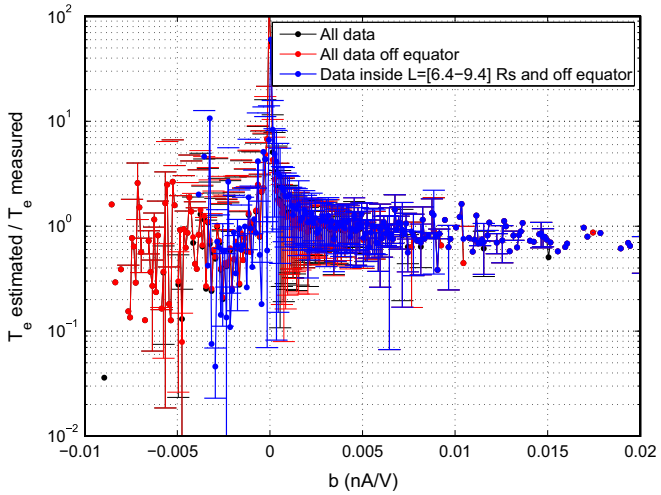

Fig. 5. Ratio between the LP estimated (derived in Section 5) and CAPS measured electron temperature as a function bins of the slope *b* of the LP current–voltage curve for negative potentials. Several selections of the whole dataset are compared, based on the spacecraft location in the magnetosphere ("off equator" refers to $|Z| > 2\ R_S$), to focus on regions where the warm electrons contribute the most to the LP current. All data points are shown and compared with the mean and standard deviation values for abscissa bins.

the large dataset, as a function of the measured *b* slope. The figure confirms that the mean ratio is close to one for large positive slope values, with a ratio at one within a factor of two (including the error bar) for $b > 2 \times 10^{-3}$ nA/V, or a ratio at one within a factor of two (excluding the error bar) for $b > 0.5/1 \times 10^{-3}$ nA/V, for any sub-selection of the large dataset. The large ratios near $b = 0$ nA/V are artificially induced by the almost infinite value of the ratio I_{ener}/b_{ener}.

However, a correlation analysis between the estimated and measured temperatures (using the data in the *L* range 6.4–9.4R_S, with $|Z| > 2R_S$ and $b > 2 \times 10^{-3}$ nA/V) reveals a limit for the T_e estimation, with a positive Pearson's correlation factor of about 0.32 only. A Fisher test (Press et al., 2007) nonetheless confirms the significance of the correlation, with a ratio between the experimental and theoretical (for 5% level of risk) Fisher statistics of 24.9: there is thus a negligible risk (probability of $\sim 1.5 \times 10^{-21}$) that the estimated electron temperature is actually independent from the measured temperature.

Despite a non-perfect correlation with the measurements, we showed that estimations of large electron temperatures may be derived in the regions where the warm electrons strongly influence the LP observations, i.e. when the electron temperature is in the range $\sim$[100–500] eV, which is observed in the *L* range 6.4–9.4R_S at Saturn and may be identified from the LP observations through large positive values of the current–voltage slope *b* ($b > 1 - 2 \times 10^{-3}$ nA/V). This not only allows us to extend the electron temperature measurement capabilities of the LP (essentially limited to $T_e < 5$ eV), but also allows us to derive small electron densities below the usual limits of the LP, as demonstrated in the next section.

6. Deriving low electron densities

This section will show how electron densities, that are lower than the usual measurement capacity of the LP, can be derived in the regions where the energetic contributions are large, based on the electron temperature estimate previously derived.

The I_{ener} and b_{ener} theoretical expressions from the moments method (Eq. (10)) correspond to a system of two linear equations with two variables being the electron moments (n_e, T_e), as soon as the maximum yield value of the LP surface is known. If we use the

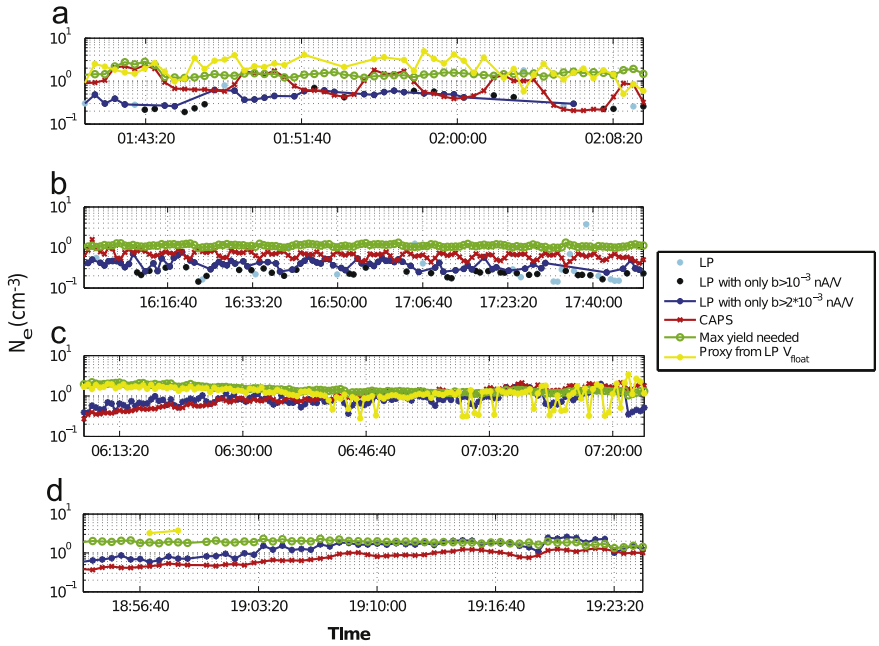

Fig. 6. Electron density n_e during several case studies: 2008 May 18, 01:40–02:10 UT (panel (a)), 2007 December 19, 16:00–17:50 UT (panel (b)), 2008 April 30, 06:08–07:25 UT (panel (c)) and 2008 May 25, 18:53–19:25 UT (panel (d)). The densities measured by CAPS ELS are compared with our estimated densities from the ion side observations of the LP (Eq. (17)) for several data selections based on the slope b values measured, and the density derived from the proxy method using the floating potential (Morooka et al., 2009). The maximum secondary electron yield needed to reproduce the I_{ener} observations during the case studies is also given.

electron temperature estimated in the previous section, we may then derive an independent estimate of the electron density in the regions where the warm electrons have a strong influence (and where the electron density is usually small compared with the classical LP measurement capability).

The electron density may thus be estimated from the $I_{ener_{moments}}$ parameter:

$$n_{e_{est}} = \frac{27 I_{ener_{moments}}}{KLA(k_B T_e/e - 37/2)} \quad (17)$$

Fig. 6 shows the resulting density estimate, assuming a maximum yield value $\delta_{e_{max}} = 1.5$ (in agreement with the values provided in Table 2 of G13) during the same four time periods as in Fig. 4. The estimated density is shown for several selections of the data (based on the slope b values), and compared with the CAPS ELS measured density. We also show the maximum yield value needed to reproduce the exact value of the energetic contribution I_{ener} at each time step (same method as for the panel (c) in Fig. 2), that may be slightly different from the 1.5 value assumed to derive the density estimate. Finally, the figure also provides the estimated density based on another technique, using a proxy between the floating potential measured by the LP and the electron density measured during the Saturn Orbit Insertion in 2004 (see Morooka et al., 2009). This technique provides small electron densities in the Saturnian magnetosphere, but several instrumental limits prevent its use at any time, leading to available proxy densities for only two of the time periods considered here (except a few data in panel (d)).

The figure reveals a good agreement between the measured and estimated densities (with $b > 1$ or 2×10^{-3} nA/V): the mean relative absolute errors are respectively of about 48% (panel (a)), 38% (panel (b)), 30% (panel (c)) and 76% (panel (d)). The largest error (panel (d)) corresponds to a period where the needed maximum yield is very stable but rather at 2 than 1.5 as assumed, and where the temporal correlation is however excellent (with Pearson's correlation coefficient of 0.88). The second largest error is given by the first time period (panel (a)), where a probably significant PAD anisotropy leads to an artificial sinusoidal evolution of the measured density (as discussed previously in Section 5); the largest difference is observed near 01:43:20 UT, where the needed maximum yield becomes unphysical (close to 3), which may reveal an overestimation of the electron density by the CAPS instrument.

Moreover, the agreement between our estimated values and the measurements is better than that between the measurements and the proxy densities, with almost a factor of 10 of difference at the beginning of the third period (panel (c)).

A statistical analysis was also performed, as previously done for the electron temperature estimate in Section 5. The ratio between the estimated and measured electron densities shows a similar behavior to Fig. 5 regarding the slope b value, with a ratio close to one for large positive slopes (not shown). Fig. 7 gives the ratio between the estimated and measured densities as a function of the estimated electron temperature (derived in Section 5), for several selections of the whole dataset (based on the slope values or the magnetospheric region) from February 1, 2005 to July 30, 2008. A very similar figure would be obtained if the measured temperature was used for the abscissa.

The figure reveals a very good agreement with the measurements in the range 100–500 eV for large positive slope values. It is neither necessary to focus on the secondary electron current region ($L = [6.4–9.4]$ R_S) off the equator nor to select only very large slope values above 2×10^{-3} nA/V to obtain a good agreement, except between 100 and 150 eV where the ratio reaches 2–3 without these combined criteria. If we consider the data inside $L = [6.4–9.4]$ R_S off the equator ($|Z| > 2$ R_S) with only $b > 2 \times 10^{-3}$ nA/V, the dispersion is smaller than one, with a mean absolute relative error below 50% above 100 eV, and of the order of 20–30% when the estimated electron temperature is in the range $\sim$150–500 eV. Moreover, the figure confirms that the proxy method (Morooka et al., 2009) leads to larger errors compared with the measurements, with a mean ratio above three and a very large standard deviation. The correlation between the measured and estimated electron densities is larger – with

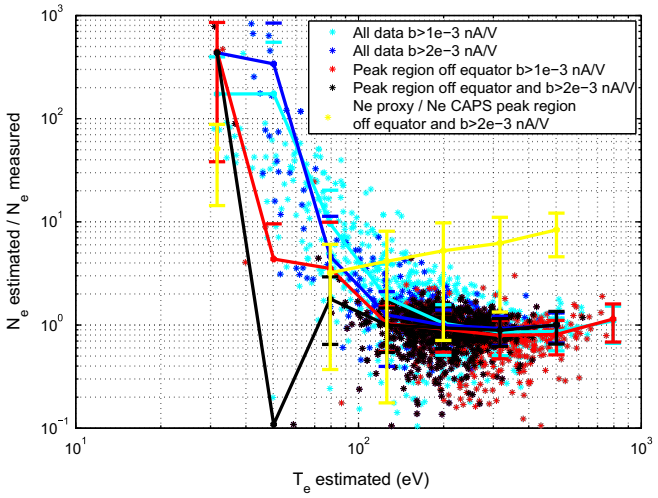

Fig. 7. Ratio between the LP estimated (Section 6) and CAPS measured electron densities as a function of the LP estimated electron temperature (derived in Section 5), for several selections of data : "peak region" refers to the L range 6.4–9.4 R_S, "off equator" refers to $|Z|>2$ R_S. All data points are shown and compared with the mean and standard deviation values for several abscissa bins. A maximum secondary electron yield of 1.75 is assumed for the figure. The mean ratio between the proxy (Morooka et al., 2009) and measured densities is also shown for the same dataset as the black points corresponding to our density estimate.

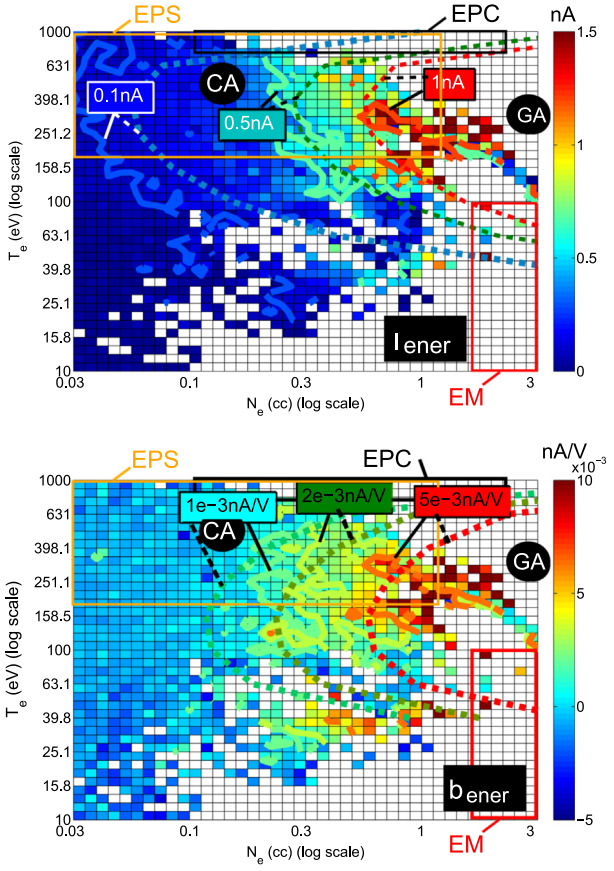

Fig. 8. Color maps of the energetic contributions I_{ener} (upper panel) and b_{ener} (lower panel) as a function of the (n_e, T_e) measurements by the CAPS ELS instrument. Six contour lines are superimposed on each panel, corresponding to three different levels (0.1/0.2/1 nA for I_{ener} and $1/2/5\times10^{-3}$ nA/V for b_{ener}) and two methods: the solid lines give the measured contours, whereas the dashed lines give the theoretical contours based on the moments approach (with $\delta_{e_{max}}=1.5$). The colors of the contour lines are slightly different from the color bar for a better viewing. The data below $n_e=0.03$ cc are not shown, since the current measured by the LP is below the noise level. The plasma regime (n_e, T_e) of other environments is also shown: "EPS" for Earth plasma sheet, "EM" for Earth magnetosheath, "EPC" for Earth plasma cavities", "CA" for Callisto and "GA" for Ganymede. See the text for the references used. (For interpretation of the references to color in this figure caption, the reader is referred to the web version of this paper.)

Pearson's correlation coefficient of 0.48 – than for the electron temperature estimation (for the data inside $L=[6.4\text{–}9.4]$ R_S off the equator with only $b>2\times10^{-3}$ nA/V). Nonetheless, the density estimate uses the temperature estimate as an input. The better density correlation is due to a smaller variability of the temperature than that of the density. Finally, for comparison, the corresponding correlation coefficient for the densities given by the proxy method is almost null (0.03).

The estimation of the electron density is thus valid over about an order of magnitude, between ~0.1 and a few cc, which enlarges the classic capabilities of the LP (limited to densities above several cc) in the regions where the energetic contributions are dominant. Moreover, our method provides a better estimation of the measured densities than the proxy method in these regions.

7. A general analysis of the influence of warm electrons

G13 showed that the warm electrons influence the LP observations when the electron temperature is between the anticritical and critical temperatures, i.e. in the range ~100–500 eV given the SEEY yield curve of the LP surface. In this range, the incident electrons generate a number of secondary electrons as well as a significant current, which itself modifies the current–voltage curve through the DC level and slope energetic contributions I_{ener} and b_{ener}. The analysis of the expressions of I_{ener} and b_{ener} from the moments approach (equation (10)) reveals, beyond the influence of the electron temperature, an influence of the electron density. The energetic contributions are indeed proportional to the electron density. A significant energetic contribution will correspond to two combined criteria on both the electron temperature (that allows the presence of more secondary than incident electrons) and density (that will reduce or enhance the energetic contributions).

This combined influence may be seen in Fig. 8, where the energetic contributions are shown as a function of both the electron temperature and density measured by CAPS ELS, for all data off the equator ($|Z|>2$ R_S) from February 1, 2005 to July 30, 2008. The current due to thermal ions may be neglected off the equator, which allows us to derive and map the energetic contributions.

The measured and theoretical contour lines are in good agreement, and show the T_e and n_e ranges that correspond to specific levels of I_{ener} or b_{ener}. The I_{ener} energetic contribution to the DC level of the I–V LP curve is thus significant (above the noise level of 0.1 nA) for densities at least above 0.03 cc, or only for larger densities when T_e is close to the theoretical anticritical or critical temperatures ($T_A\sim35$ eV and $T_c\sim1030$ eV for $\delta_{e_{max}}=1.5$). The b_{ener} contribution shows the same behavior, with however a lesser influence of the electron temperature with contour lines more flat (as expected from Eq. (15)). The 1×10^{-3} nA/V b_{ener} level, i.e. the minimum value to derive LP estimations of the electron temperature and density (see Sections 5 and 6), corresponds to n_e values at least above 0.1 cc.

Beyond the absolute value of the energetic contributions, it is important to estimate their relative importance compared with the thermal ion contribution to conclude on their impact on the LP observations in a specified plasma region. As a consequence, we calculated the ratios I_{ener}/I_{i0} and b_{ener}/b_{ions} from the following

equations:

$$\begin{cases} I_{ener_{moments}} = \dfrac{An_eKL\left(\dfrac{k_BT_e}{e} - 37/2\right)}{27} \\ b_{ener_{moments}} = -\dfrac{An_eKL}{27} \end{cases} \tag{18}$$

and

$$\begin{cases} I_{i_0} = -\sum_i A_{LP} q_i n_i \sqrt{\dfrac{v_i^2}{16} + \dfrac{k_BT_i}{2\pi m_i}} \\ b_{ions} = -\sum_i A_{LP} q_i n_i \sqrt{\dfrac{v_i^2}{16} + \dfrac{k_BT_i}{2\pi m_i}} \dfrac{e}{m_i v_i^2/2 + k_BT_i} \end{cases} \tag{19}$$

If we assume a single ion species and $n_i = n_e$ then the ratios I_{ener}/I_{i0} and b_{ener}/b_{ions} will depend only on T_e, m_i (ion mass), v_i (ion drift velocity) and T_i (ion temperature) since n_e disappears. It is thus possible to plot both ratios in Fig. 9 as a function of respectively (T_e, Wi_{eff}) and (T_e, Wi_{eff2}), where

$$\begin{cases} Wi_{eff} = \dfrac{v_i^2}{16} + \dfrac{k_BT_i}{2\pi m_i} \\ Wi_{eff2} = \sqrt{Wi_{eff}} \dfrac{e}{m_i v_i^2/2 + k_BT_i} \end{cases} \tag{20}$$

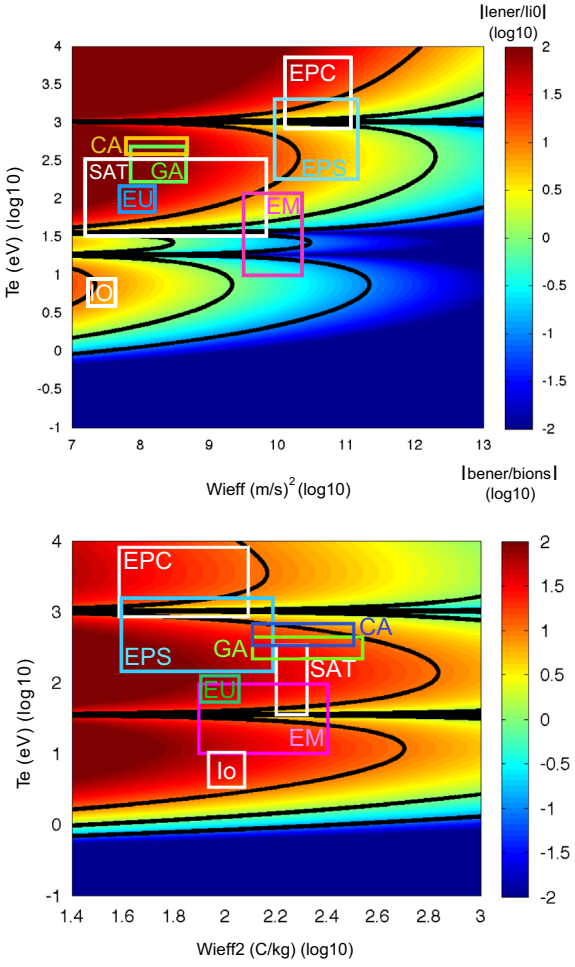

Fig. 9. Color maps of the modeled ratios between the energetic contributions and the thermal ion contributions to the DC level (upper panel) and slope (lower panel) of the negative potentials side of the LP I–V curve. The contours (black solid lines) show three different ratio levels (0.1/1/10) to reveal where the energetic contributions dominate or not versus the ion contributions. (Upper panel) The ratio I_{ener}/I_{i0} – where I_{i0} is the random ion current – is given as a function of the electron temperature and of an ion parameter *Wieff* that contains the ion plasma conditions. (Lower panel) The ratio b_{ener}/b_{ions} is given as a function of T_e and $Wieff_2$. The plasma conditions of other environments are shown (same as Fig. 8, with also Io and "EU" for Europa). See text for more details. (For interpretation of the references to color in this figure caption, the reader is referred to the web version of this paper.)

Fig. 9 shows that the energetic contributions I_{ener} and b_{ener} may often be the main contributor of the LP currents measured for negative potentials (assuming that the photoelectron current has been properly removed). The ion temperature/velocity (through Wi_{eff} and Wi_{eff2}) will differently impact the two ratios: large ion temperatures/velocities will induce a large slope ratio but a small DC-level ratio. Besides, only absolute values are provided, since the ratios are negative in the range 35–1000 eV. We must add that the ratio I_{ener}/I_{i0} is not realistic around 37/2, where it unphysically reduces to 0 (which is due to our approximation using a simple Boltzmann distribution function).

Figs. 8 and 9 allow us to predict the importance of the energetic contributions to LP observations in any plasma environment whose characteristics are known. Several planetary environments (at Earth or Jupiter) are superimposed on the graphs, showing the expected energetic contributions if the same probe was used in these regions. The plasma characteristics for the environment of galilean satellites were taken from Table 21.1 in Bagenal et al. (2004), those of Earth plasma cavities were taken from McFadden et al. (1999), while the typical Earth plasmasheet and magnetosheath characteristics were taken from several references (Christon et al., 1989; Tsyganenko, 2003; Culot, 2001). As a consequence, warm electrons may impact LP observations in a large variety of plasma environments of the solar system. In particular, the ratios I_{ener}/I_{i0} and b_{ener}/b_{ions} are large enough (essentially larger than 10) in the regions of Ganymede/Callisto/Europa to suggest the possibility to derive the large electron temperature and low electron density of their surrounding plasma with the future Langmuir probes planned for the JUICE mission.

This analysis of the relative importance of energetic plasma contributions to LP observations for negative potentials is a general result that may be easily adapted for other LPs that may have a different sweep voltage ([−32 V +32 V] for Cassini), or a different maximum secondary electron yield (due to a different surface composition or treatment).

8. Conclusions

Though Langmuir probes (LP) are designed to investigate cold plasma regions (e.g. ionospheres), Garnier et al. (2012) revealed a strong sensitivity of the Cassini LP measurements to hundreds of eV electrons. These warm electrons impact the surface of the probe and generate a significant current of secondary electrons, that is mostly observed in the dipole L Shell range of ~6–10 in the magnetosphere. Garnier et al. (2013) then showed that both the DC level and the slope of the current–voltage curve of the LP (for negative potentials) are influenced by these warm electrons, through respective contributions called I_{ener} and b_{ener} that may be modeled through several approaches with a reasonable precision.

This paper shows how we can derive information about the incident warm electrons, from the analysis of the energetic contributions I_{ener} and b_{ener} to the current–voltage curve. First, modeling the energetic contributions allows us to provide information about the pitch angle anisotropies of the incident hundreds of eV electrons (Figs. 2 and 3). The LP alone cannot provide any information about the pitch angle distribution (PAD) of the electrons, but it can through the modeling of I_{ener} and b_{ener}. This modeling, based on the incident electron distribution function

given by the single anode 5 of the CAPS ELS instrument, reveals large dispersions of the estimated maximum secondary electron yield (which is a constant for a surface material) needed to reproduce the observed I_{ener}/b_{ener}. Such dispersions give evidence for strong pitch angle anisotropies of the incident electrons, and using a functional form of the PAD may even allow us to derive the real peak angle of the PAD.

Second, rough estimates of the electron temperature may be derived (Eq. (16), Figs. 4 and 5) in the regions where the warm electrons strongly influence the LP observations, i.e. when the electron temperature is in the range $\sim$[100–500] eV. These estimates may be derived essentially in the L range 6.4–9.4 R_S at Saturn and may be identified from the LP observations through large positive values of the current–voltage slope b ($b>1$ or 2×10^{-3} nA/V). The estimated temperature values lie far beyond the classical measurement capabilities of the LP (<5 eV for Cassini). Future work will be however needed to refine the temperature derivation to obtain a larger correlation coefficient with the CAPS measurements.

The estimated temperature may then be used to derive the associated electron density in the regions where the energetic contributions are dominant (Eq. (17), Figs. 6 and 7). Both case studies and a statistical analysis show a good correlation with the CAPS derived values, with estimated densities between $\sim$0.1 and a few cc (below the classical capabilities of the LP which measures essentially $n_e>5$ cc). Moreover, our method provides a better estimation of the electron density in these regions than the proxy method based on the floating potential of the LP (Morooka et al., 2009).

Such electron density and temperature estimates may be obtained during many time intervals of the Cassini mission, corresponding to 61 days among the 3.5 years of observations considered and to a large fraction of the intervals when Cassini was located off the equator in the L range 6.4–9.4 R_S. This approximate derivation technique may be all the more useful since the shutdown of the CAPS instrument that was the main provider of electron moments in Saturn's magnetosphere. The method developed in the paper can provide useful information about the electron moments (for $\sim$[100–500] eV electrons), and even provide probably better estimates than CAPS in some cases (when the plasma is strongly anisotropic and when the anode 5 is not properly oriented) but it cannot replace in general the CAPS instrument.

Finally, we use the simple approach provided by the moments method of Garnier et al. (2013) to predict the impact of the energetic contributions on LP measurements in any plasma environment (Figs. 8 and 9). The I_{ener} and b_{ener} contributions and their relative importance compared with the ambient ions contribution may be indeed calculated for any plasma region whose characteristics (density, temperature, etc.) are known. This reveals that LP observations may be influenced by warm electrons in several planetary plasma regions in the solar system, and that ambient magnetospheric electron density and temperature could be estimated in some of them, e.g. around several galilean satellites, through the use of Langmuir probes.

Acknowledgments

We would like to thank M. Morooka and S. Rochel for their help. This work was done with the support of CNES.

References

Ågren, K., Edberg, N., Wahlund, J.-E., 2012. Detection of negative ions in the deep ionosphere of titan during the Cassini T70 flyby. Geophys. Res. Lett. 39, L10201. http://dx.doi.org/10.1029/2012GL051714.

Ågren, K., et al., 2007. On magnetospheric electron impact ionisation and dynamics in Titan's ram-side and polar ionosphere—a Cassini case study. Ann. Geophys. 25, 2359–2369. http://dx.doi.org/10.5194/angeo-25-2359-2007.

Bagenal, F., Dowling, T., McKinnon, W., 2004. Jupiter. The Planet, Satellites and Magnetosphere. Cambridge University Press, Cambridge.

Baglin, V., Bojko, J., Grbner, O., Henrist, B., Hilleret, N., Scheuerlein, C., Taborelli, M., 2000. The secondary electron yield of technical materials and its variation with surface treatments. In: Proceedings of EPAC 2000, Vienna, Austria, pp. 217–221.

Christon, S., Williams, D., Mitchell, D., 1989. Spectral characteristics of plasma sheet ion and electrons populations during undisturbed geomagnetic conditions. J. Geophys. Res. 94, http://dx.doi.org/10.1029/JA094iA10p13409 13,409–13,424.

Culot, F., 2001. The Earth's Magnetosphere Plasma Boundaries (Master thesis report). CETP, Paris.

DeJong, A., Burch, J., Goldstein, J., Coates, A., Crary, F., 2011. Day-night asymmetries of low-energy electrons in Saturn's inner magnetosphere. Geophys. Res. Lett. 38, L08106. http://dx.doi.org/10.1029/2011GL047308.

Edberg, N., et al., 2011. Structured ionospheric outflow during the Cassini T55–T59 Titan flybys. Planet. Space Sci. 59, 788–797. http://dx.doi.org/10.1016/j.pss.2011.03.007.

Edberg, N., et al., 2013. Extreme densities in Titan's ionosphere during the T85 magnetosheath encounter. Geophysical Research Letters 40 (12), 2879–2883.

Fahleson, U., Fälthammar, C.-G., Pedersen, A., 1974. Ionospheric temperature and density measurements by means of spherical double probes. Planet. Space Sci. 22, 41–66. http://dx.doi.org/10.1016/0032-0633(74)90122-6.

Garnier, P., Holmberg, M., Lewis, G., Thomsen, M., Grimald, S., Gurnett, D., Coates, A., Crary, F., Dandouras, I., 2013. The influence of the secondary electrons induced by energetic electrons impacting the Cassini Langmuir probe at Saturn. J. Geophys. Res. 118, 1–20. http://dx.doi.org/10.1002/2013JA019114.

Garnier, P., et al., 2009. Titan's ionosphere in the magnetosheath: Cassini RPWS results during the T32 flyby. Ann. Geophys. 27, A10202. http://dx.doi.org/10.1029/2011JA017298.

Garnier, P., et al., 2012. The detection of energetic electrons with the Cassini Langmuir probe at Saturn. J. Geophys. Res. 117, A10202. http://dx.doi.org/10.1029/2011JA017298.

Gurnett, D., et al., 2004. The Cassini radio and plasma wave investigation. Space Sci. Rev. 114, 395–463. http://dx.doi.org/10.1007/s11214-004-1434-0.

Gustafsson, G., Wahlund, J.-E., 2010. Electron temperatures in Saturn's plasma disc. Planet. Space Sci. 58, 1018–1025. http://dx.doi.org/10.1016/j.pss.2010.03.007.

He, P., Hseuh, H.C., Mapes, M., Todd, R., Weiss, D., 2001. Development of titanium nitride coating for SNS ring vacuum chambers. In: Proceedings of the 2001 IEEE Particle Accelerator Conference, Chicago, pp. 2159–2161.

Holmberg, M., Wahlund, J.-E., Morooka, M., 2012. Ion densities and velocities in the inner plasma torus of Saturn. Planet. Space Sci. 73, 151–160. http://dx.doi.org/10.1016/j.pss.2012.09.016.

Lai, S.T., Tautz, M., 2008. On the anticritical temperature for spacecraft charging. J. Geophys. Res. 113, A11211. http://dx.doi.org/10.1029/2008JA013161.

Lewis, G., Andre, N., Arridge, C., Coates, A., Gilbert, L., Linder, D., Rymer, A., 2008. Derivation of density and temperature from the Cassini–Huygens CAPS electron spectrometer. Planet. Space Sci. 56, 901–912. http://dx.doi.org/10.1016/j.pss.2007.12.017.

Lorkiewicz, J., Kula, J., Pszona, S., Sobczak, J., Bilinski, A., 2007. Sublimation TiN coating of RF power components. In: Proceedings of AIP International Conference on Research and Applications of Plasmas, vol. 993, pp. 411–414. http://dx.doi.org/10.1063/1.2909163.

McFadden, J., Carlson, C., Ergun, R., Klumpar, D., Moebius, E., 1999. Ion and electron characteristics in auroral density cavities associated with ion beams: No evidence for cold ionospheric plasma. J. Geophys. Res. 104, http://dx.doi.org/10.1029/1999JA900035 14,671–14,682.

Morooka, M.W., et al., 2009. The electron density of Saturn's magnetosphere. Ann. Geophys. 27, 2971–2991. http://dx.doi.org/10.5194/angeo-27-2971-2009.

Morooka, M.W., et al., 2011. Dusty plasma in the vicinity of enceladus. J. Geophys. Res. 116, A12221. http://dx.doi.org/10.1029/2011JA017038.

Mott-Smith, H.M., Langmuir, I., 1926. The theory of collectors in gaseous discharges. Phys. Rev 28, 727–763. http://dx.doi.org/10.1103/PhysRev.28.727.

Press, W.H., Teukolsky, S.A., Vetterling, W.T., Flannery, B.P., 2007. Numerical Recipes: The Art of Scientific Computing, 3rd ed. Cambridge University Press, Cambridge, United Kingdom.

Rymer, A., Mauk, B., Hill, T., Paranicas, C., Mitchell, D., Coates, A., Young, D., 2008. Electron circulation in Saturns magnetosphere. J. Geophys. Res. 113, A01201. http://dx.doi.org/10.1029/2007JA012589.

Sakai, S., Watanabe, S., Morooka, M., Holmberg, M., Wahlund, J.-E., Gurnett, D., Kurth, W., 2013. Dust-plasma interaction through magnetosphere-ionosphere coupling in saturn's plasmadisk. Planet. Space Sci. 75, 11–16. http://dx.doi.org/10.1016/j.pss.2012.11.003.

Sanders, N.L., Inouye, G.T., 1978. Secondary emission effects on spacecraft charging: energy distribution consideration. In: Finke, R.C., Pike, C.P. (Eds.), Spacecraft Charging Technology 1978. U.S. Air Force Geophysics Lab., Hanscom, MA, pp. 747–755.

Sittler, E., et al., 2008. Ion and neutral sources and sinks within Saturn's inner magnetosphere: Cassini results. Planet. Space Sci. 56, 3–18. http://dx.doi.org/10.1016/j.pss.2007.06.006.

Tsyganenko, N., 2003. Tail plasma sheet models from geotail particle data. J. Geophys. Res. 108, 1136. http://dx.doi.org/10.1029/2002JA009707.

Wahlund, J., et al., 2005a. Cassini measurements of cold plasma in the ionosphere of titan. Science 308, 986–989. http://dx.doi.org/10.1126/science.1109807.

Wahlund, J.-E., et al., 2005b. The inner magnetosphere of Saturn: Cassini RPWS cold plasma results from the first encounter. Geophys. Res. Lett. 32, L20S209. http://dx.doi.org/10.1029/2005GL022699.
Wahlund, J.-E., et al., 2009. Detection of dusty plasma near the E-ring of Saturn. Planet. Space Sci. 57, 1795–1806. http://dx.doi.org/10.1016/j.pss.2009.03.011.
Walters, D., Ma, Q., 2001. Secondary electron yield of a thin film coating on the APS RF cavity tuners. In: Proceedings of the 2001 IEEE Particle Accelerator Conference, Chicago, pp. 2153–2155.
Young, D., et al., 2004. Cassini plasma spectrometer investigation. Space Sci. Rev. 114, 1–112. http://dx.doi.org/10.1007/s11214-004-1406-4.